MODELLING THE BEHAVIOUR OF STEEL-FIBRE REINFORCED CONCRETE GROUND SLABS I: DEVELOPMENT OF MATERIAL MODEL

Elsaigh, W.A., Robberts, J.M., and Kearsley, E.P.

Pretoria University

Abstract

Steel Fibre Reinforced Concrete (SFRC) brings favourable properties to concrete ground slabs. The use of the material is limited by the lack of an appropriate analysis method. This paper is the first in a series of two regarding research aimed at providing a modelling approach, which can be used to model the behaviour of SFRC concrete and SFRC ground slabs. Here, an improved generalized analytical method is presented to determine the tensile stress-strain (σ-ε) response using an inverse analysis. The tensile σ-ε response is determined using either the experimental moment-curvature (M-ϕ) or load-deflection (P-δ) responses. The validity of the inverse analysis is evaluated by comparing calculated and measured tensile σ-ε responses. The tensile σ-ε response is subsequently utilized in nonlinear finite element analysis of a SFRC beam with the purpose of examining the tensile σ-ε relationship. The calculated results compare well with the experimental observations.

Contact details

Corresponding author	Dr. W. A. Elsaigh,	Tel: +27 12 420 4129	whelsaigh@yahoo.com
Co-author	Dr. J. M. Robberts	Tel: +27 11 234 7654	john.robberts@nucse.com
Co-author	Prof. E. P. Kearsley	Tel: +27 12 420 2176	elsabe.kearsley@eng.up.ac.za

Introduction

Steel Fibre Reinforced Concrete (SFRC) is a composite material consisting of a concrete matrix containing a random dispersion of steel fibres. A comparison between SFRC and counterpart plain concrete shows that SFRC exhibits superior mechanical properties, such as increase in total energy absorption prior to complete separation (Johnston, 1985), improved fatigue resistance (Johnston and Zemp, 1991), larger impact strength (Banthia et al., 1995) and higher shear strength (Jindal, 1984, Minelli and Vecchio, 2006). The improvement of the mechanical properties of SFRC can be attributed to the localized reinforcing effect of steel fibres, enhanced by either (a) resistance to crack extension provided near a crack tip as steel fibres possess much higher strength compared to their surrounding concrete (Parker, 1974), or (b) crack bridging effect due to steel fibres transmitting stresses across the crack (Bekaert, 1999). Consequently, the localized reinforcing capability of steel fibres is greatly dependent on fibre-matrix interaction as well as the steel fibre properties (i.e., texture, strength and end shape), content, and orientation with respect to the direction of crack propagation.

Since steel fibres are mostly effective upon cracking, analysis aiming at ultimate load-carrying capacity needs to proceed beyond the initial cracking stress of the material. Such an analysis may be performed by utilizing non-linear finite element methods (NLFEM). A proper representation of concrete cracking behaviour and an appropriate constitutive material law are the most essential aspects for a successful non-linear finite element analysis (NLFEA). The smeared crack approach, widely used to study the cracking behaviour of conventionally reinforced concrete, can effectively be incorporated to analyze SFRC. In the smeared crack approach, a crack is considered as an infinite number of parallel fissures across a specified part of the finite element (FE). Based on the state of the crack, different formulations are available for the smeared crack approach including: single-fixed crack, rotating crack and multiple fixed crack.

Several methods were proposed in literature to determine the tensile stress-strain (σ-ε) response of the SFRC. Lim et al. (1987a and b) developed a tensile σ-ε response using laws of mixture and results from steel fibre pullout tests. The response of a volume-weighted sum of concrete and steel fibres was used to determine the SFRC behaviour. The post-cracking strength was

determined using the ultimate pullout bond strength. Using laws of mixture to determine the pre-peak behaviour for concrete with relatively low steel fibre contents have been criticized by Soroushian and Bayasi (1987) who considered the effect of steel fibres at this stage to be negligible. A kin method, with some modification, was also adopted by Lok and Xiao (1998). Nemegeer (1996) and RILEM TC 162-TDF (2002) proposed a tensile σ-ε response that uses results from a deformation-controlled beam-bending test to determine the peak and post-cracking stresses. In the RILEM TC 162-TDF (2002) method, strains corresponding to these stresses were empirically estimated as fixed values. The main shortcoming of the RILEM tensile σ-ε response lies in the accuracy of the procedure used to determine the load at initiation of the crack on a measured load-deflection (P-δ) response, not to mention, the assumptions made for the calculation of the post-cracking strength (Tlemat et al., 2006).

The availability of steel fibres with a variety of physical and mechanical properties, as well as the use of a range of fibre contents, tend to complicate the determination of the tensile σ-ε response of SFRC. The further complexities of testing concrete in direct tension and measuring stresses and strains may be the reasons for the many proposed material models. The current international drive for establishing tensile σ-ε relationships for SFRC has, however, shifted towards inverse analysis, i.e., backcalculation, techniques. In these techniques the flexural response obtained from beam-bending tests is used to backcalculate the tensile σ-ε relationship. Elsaigh et al. (2004) proposed a method to determine the tensile σ-ε relationship for SFRC utilising experimental results obtained from beam third-point tests. Alena et al. (2004) have concurrently proposed a similar method. Østergaard and Olesen (2005) and Østergaard et al. (2005) have also proposed an inverse analysis method based on the so called “non-linear hinge concept” initially described by Olesen (2001). The merit of the inverse analysis procedures is that they require measured M-ϕ or P-δ responses obtainable with minimal testing complexities compared to procedures requiring results from direct tensile tests. In addition, these methods adopt a macro approach since the influence of the steel fibre parameters and the concrete matrix are reflected in the measured M-ϕ or P-δ responses. This is an advantage compared to procedures utilising a micro approach in which the fibre properties, the concrete matrix characteristics and the fibre-matrix interaction have to be known.

This paper is the first in a series of two regarding research conducted by Elsaigh (2007) aimed at providing a modelling approach that can be used to analyze SFRC ground slabs and eventually promote the material use in concrete pavements. The main objective of this paper is to propose and verify a modified inverse analysis method that can be used to determine the tensile σ-ε response for SFRC. In the method, proposed by Elsaigh et al. (2004), it was postulated that the deflection of a simply supported beam is only due to bending stresses and the effect of shear stresses was not considered. This is because their effect on deflection of beams is usually relatively small compared to the effects of flexural deformations. However, for beam specimens of the type normally specified for laboratory testing, the span-depth ratio lies in the range of 3 to 4 and therefore shear stresses will contribute significantly to the total deflections of the beam. The modified method, taking the effect of shear stresses into account, will be briefly described here while the back-calculated tensile σ-ε response and results obtained from NLFEA of the beam will be used in a subsequent analysis involving a SFRC ground slab manufactured using similar material as in the beam. The analyzes of the SFRC ground slab will be presented in a separate paper.

Inverse Analysis method

In the analysis the M-ϕ and the P-δ responses are derived by assuming a σ-ε response. A trial and error technique is followed, by adjusting the σ-ε relationship until the analytical results fit the experimental results for either M-ϕ or P-δ. In the analysis, the following three-step procedure is used to calculate the P-δ response of SFRC beams:

(1) Assume a σ-ε relationship for the SFRC.

(2) Calculate the M-ϕ response for a section; and

(3) Calculate the P-δ response for an element.

At the end of either steps (2) or (3) the results from the analysis are compared to experimental results and adjustments are made to the σ-ε response until the analytical and experimental results agree within acceptable limits.

Proposed stress-strain relationship

The shape of the proposed σ-ε relationship used in this analysis is shown in Fig. 1. σ_{t0} and ε_{t0} represents the cracking strength and the corresponding elastic strain. σ_{tu} and ε_{t1} represents the residual stress and the residual strain at a point where the slope of softening tensile curve changes. ε_{tu} is the ultimate tensile strain. E is Young's modulus for the SFRC. σ_{cu} and ε_{co} are the compressive strength and the analogous elastic strain. ε_{cu} is the ultimate compressive strain. The proposed tensile response is similar in shape to that proposed by RILEM TC 162-TDF (2002) while the compression response is assumed linear elastic up to a limiting strain ε_{c0} while assumed ideally plastic beyond this value. The mathematical form of the σ-ε relationship is expressed as follows:

$$\sigma(\varepsilon) = \begin{cases} \sigma_{cu} & \text{for } (\varepsilon_{cu} \le \varepsilon < \varepsilon_{c0}) \\ E\,\varepsilon & \text{for } (\varepsilon_{c0} \le \varepsilon < \varepsilon_{t0}) \\ \sigma_{t0} + \psi\,(\varepsilon - \varepsilon_{t0}) & \text{for } (\varepsilon_{t0} \le \varepsilon < \varepsilon_{t1}) \\ \sigma_{tu} + \lambda\,(\varepsilon - \varepsilon_{t1}) & \text{for } (\varepsilon_{t1} \le \varepsilon < \varepsilon_{tu}) \end{cases} \qquad (1)$$

Where: $E = \dfrac{\sigma_{cu}}{\varepsilon_{c0}}$, $\psi = \dfrac{\sigma_{tu} - \sigma_{t0}}{\varepsilon_{t1} - \varepsilon_{t0}}$; and $\lambda = \dfrac{-\sigma_{tu}}{\varepsilon_{tu} - \varepsilon_{t1}}$

Moment-curvature response

The M-ϕ relationship at a section is calculated by assuming (a) the σ-ε relationship of the material is known; (b) plane sections perpendicular to the centre plane in the reference state remain plane during bending; and (c) internal stress resultants are in equilibrium with the externally applied loads.

As part of the first assumption, the σ-ε relationship proposed in equations (1) is used and initial values are assumed for the parameters. The second assumption applies to slender beams and implies a linear distribution of strain so that the following relationships exist at a section (see Fig.2b):

$$\varepsilon(y) = \frac{y}{a}\varepsilon_{top} = \left(\frac{y}{h-a}\right)\varepsilon_{bot} \qquad (2)$$

The final assumption is used to find the axial force F (which is equal to zero) and moment M (which is equal to the applied moment):

$$F = \int_{-(h-a)}^{a} \sigma(\varepsilon)\, b\, dy = \frac{a\, b}{\varepsilon_{top}} \int_{\varepsilon_{bot}}^{\varepsilon_{top}} \sigma(\varepsilon)\, d\varepsilon = 0 \qquad (3)$$

$$M = \int_{-(h-a)}^{a} \sigma(\varepsilon)\, y\, b\, dy = -\frac{a^2 b}{\varepsilon_{top}^2} \int_{\varepsilon_{bot}}^{\varepsilon_{top}} \sigma(\varepsilon)\, \varepsilon\, d\varepsilon \qquad (4)$$

At a typical section there are two unknowns necessary to describe the strain distribution. For a given strain distribution the stresses at a section (see Fig.2c) can be calculated using the σ-ε relationship and equations (3) and (4) can be used to solve the two unknowns. The curvature at a section is given by:

$$\phi = \frac{\varepsilon_{top}}{a} = \frac{\varepsilon_{bot}}{(h-a)} \qquad (5)$$

The following procedure is followed to obtain the M-ϕ relationship:

(1) A value is selected for the bottom strain ε_{bot}.

(2) The top strain ε_{top} is solved from equation (3) by following an iterative procedure in which ε_{top} is changed until $F = 0$.

(3) M and ϕ is calculated from equations (4) and (5), respectively. This produces one point on the M-ϕ diagram.

(4) A new ε_{bot} is selected and steps (1) to (3) are repeated to until sufficient points have been generated to describe the complete M-ϕ relationship.

Load-deflection response

The total deformation of a beam consists of two components: extension caused by the moments (ε.dx) and shear distortion (γ.dx) caused by the shear force (Refer to Fig.3). At any loading point during the loading process, the total deflection of a beam (δ) is estimated as the sum of the deflection due to moments (δ_m) and the deflection due to shear forces (δ_V). The unit-load method is used to obtain the total deflection by integrating curvature ($\phi = M/EI$) and shear strain ($\gamma = V.f_{sh}/GA$) along the beam (Refer to equation 6). EI is the flexural rigidity and GA/f_{sh} is the shearing rigidity of the beam (Gere and Timoshenko, 1991).

$$\delta = \delta_m + \delta_V = \int_0^L \frac{M_u M_L .dx}{EI} + \int_0^L \frac{V_u V_L .dx}{GA/f_{sh}} \qquad (6)$$

The deflections (δ_m) due to moments are calculated from the distribution of the curvature (ϕ) due to moment along the beam, where ϕ replaces $\frac{M_u}{EI}$ in equation (6). Consider the beam in Fig.4b subjected to a variable load *P*. For moments up to the maximum moment M_m the curvature is obtained from the *M*-ϕ relationship in Fig.4a yielding the dashed line in Fig.4b. Beyond this point the analysis effectively switches to displacement control. It is assumed that material having reached M_m (part BC of the beam) will follow the softening portion of the *M*-ϕ relationship. For example; if the curvature in BC increases to ϕ_c, the moment will reduce to M_c. Equilibrium requires the moments in parts AB and CD of the beam to reduce and the material here is assumed to unload elastically, producing smaller curvatures for these parts. This is because tensile stresses on the end thirds of the beam decrease as the crack width in the middle third increases.

The deflections (δ_V) due to shear forces were calculated from the distribution of shear strain (γ) along the beam. Referring to the load configurations shown in Fig.5b, the shear deflection in the beam is due to the shear forces in part AB and CD. The fact that these two parts unload elastically at the onset of the flexural cracks in part BC has resulted in less complexities compared to that followed for the *M*-ϕ analysis. At any stage throughout the loading process of the beam, shear strains on the $V - \gamma$ response shown in Fig.5a were calculated using the measured *P*-δ response by dividing the shear force by the shearing rigidity. This means that the effect of shear forces on deflection increases to reach the maximum at the peak load and decreases with increasing displacement beyond this peak load. The distribution of elastic shear strain (γ) through the depth of beams with uncracked rectangular sections is parabolic. As a result of shear strains, cross-sections of the beam that were originally plane surfaces become warped. For the beam setup in Fig.4b and Fig.5b, the shear deformation is zero in the constant moment zone (BC). For this reason, it is justifiable to use the bending formula derived for pure bending. The effects due to shear and moment were calculated separately. The superposition concept was used to calculate the total deflection as the sum of both effects.

It is generally accepted that the area under the tensile σ-ε curve represents the fracture energy. The characteristics of the softening part of the tensile σ-ε curve is largely dependent on the size of the element in which the crack occurs. When calculating the P-δ response using the method presented here, the beam was divided into three elements and the crack was smeared over the constant moment zone (part BC of the beam). It was also assumed that an infinite number of layers (elements) exist through the depth of the beam. Therefore element size should carefully be selected when using the calculated tensile σ-ε curve in FEA. The proposed method is numerically demanding and therefore most suitable for computer applications. The numerical solution capabilities of programs such as Mathcad (2001) can greatly assist in the implementation of the method.

Validation of the analysis method

The experimental results obtained by Lim et al. (1987 a and b) are used to test the proposed analysis method. In their experimental work, they tested SFRC specimens in compression, direct tension and flexure. Results of specimens containing 0.5 percent by volume (40 kg/m^3) of hooked-end steel fibres, with 0.5 mm diameter and 30 mm length, are discussed here. The average compressive strength and Young's modulus for the SFRC were determined as 34 MPa and 25.4 GPa, respectively.

The shape of the tensile σ-ε relationship is assumed as in Fig.1. The first estimation of for σ_{t0}, ε_{t0}, σ_{tu}, ε_{t1}, and ε_{tu} is made based on the results of parameter study conducted by Elsaigh et al. (2004). A trial-and-error procedure is followed to adjust these parameters until the calculated M-ϕ and P-δ responses match the experimental responses. Fig.6 shows the tensile σ-ε relationships determined using the analysis method compared to measured response from a direct tension test. It is worth noting that no experimental data were recorded immediately beyond the maximum tensile stress.

Fig.7 shows the correlations between calculated and experimental M-ϕ and P-δ responses. The point where the maximum tensile stress (2.8 MPa) in the material is first reached occurs in the pre-peak regions of both the M-ϕ and P-δ responses (see the arrows of Fig.7). This means that to

utilize the full tensile capacity of the material, the analysis should incorporate the non-linear material properties.

Fig.8 shows the comparison between tensile σ-ε relationships, developed using the various models proposed by Lim et al. (1987 a), Nemegeer (1996) and Lok and Xiao (1998), to determine the tensile σ-ε relationship for the SFRC tested by Lim et al. (1987a). The comparison excluded the models developed by Vandewalle (2003) and Dupont and Vandewalle (2003), as they require results from notched beams test. The main difference between these four models is the value of the residual strain (ε_{t1}). The assumption made in the model of Lim et al. (1987 a) where ε_{t1} is equal to the cracking strain (ε_{t0}) resulted in a larger divergence between the experimental and calculated M-ϕ response in the region immediately beyond the maximum moment. The higher value for σ_{tu} determined using the model developed by Nemegeer (1996) resulted in an increased moment for the last part of the M-ϕ response. The results indicate improved correlation between measured and backcalculated tensile σ-ε and M-ϕ responses.

Finite element analysis of the beam

The analyzes carried out in this section utilize the experimental results for SFRC beams obtained by Elsaigh (2001). SFRC was manufactured by adding 15 kg/m^3 of steel fibres to the concrete. The steel fibres used in this investigation were hooked-end wires with an aspect ratio (length/diameter) of 80, a length of 60 mm and a tensile strength of 1100 MPa. The average Young's modulus and cube strength for the concrete were 28 GPa and 45 MPa, respectively. Three SFRC beam specimens, measuring 150 x 150 x 750 mm, were cast and water cured for 28 days before testing. The beams were supported to span 450 mm and subjected to a third-point displacement-controlled load. The beam dimensions and the supported span length results in a span to depth ration of 3, consequently, the contribution of shear stresses, analogous to maximum load, is approximately 18 percent of the total deflection. MSC.Marc (2003), a general-purpose FEA programme, was used to analyze a SFRC beam with material properties and P-δ responses as experimentally established. The FEA programme has the capability to analyze SFRC structures by utilising the cracking model for low-tension materials. This cracking model adopts single fixed crack formulations. A cracking subroutine is used to enable the input of a bilinear softening curve.

Geometry and boundary conditions

Because of symmetry, only a half of the beam is analyzed. Element type 75 of MSC.Marc (2003) is used. It is a four-node thick shell element with six degrees of freedom per node: those are three displacements (Δ_X, Δ_Y and Δ_Z) and three rotations (θ_X, θ_Y and θ_Z). The thickness is divided into an odd number of layers, with stress and stiffness states calculated at representative points through the thickness. Eleven layers were used for this analysis based on results from preliminary runs of the model. The boundary conditions and the geometry are shown in Fig.9. The geometry of the beam is generated using an element size of 150 x 150 mm and 150 x 75 mm in the left and right sides of the applied load, respectively.

The displacement-controlled loading was simulated by applying incremental displacements. The "time curve" concept available in MSC.Marc (2003) was used to ramp the applied displacement from zero to -5 mm in one time unit. The time unit was subdivided into a number of time steps, which determine the magnitude of the applied displacement increment. The magnitude of the time step was varied during the analysis to ensure that the resulting P-δ response in the post-cracking region is captured sufficiently. For example: smaller displacement increments were specified at points in the σ-ε response where the slope changes.

Material model

The average (or smeared) σ-ε response is determined for an element size of 150 x 150 mm (i.e. the crack is smeared over the middle part of the beam). The crack initiation is governed by the maximum tensile stress criterion, i.e, when the maximum principal tensile stress exceeds the cracking strength, a crack is formed. The occurrence of a crack in a particular direction is assumed not to affect the tensile strength of the material for stresses parallel to the crack. The tensile strength in a particular direction reduces based on the softening part of the tensile σ-ε response. Based on the single-fixed crack formulations provided in the MSC.Marc (2003), the orientation of the crack will be fixed throughout the analysis as soon as the material reaches the value of σ_{t0}. The adopted σ-ε relationship as well as the calculated P-δ responses are shown in Fig.10. Close agreement is found between the analytical and experimental P-δ responses.

The fracture energy for the elements having a width of 150 mm is the product of the area under the softening part of the tensile σ-ε curve and the crack smearing width (150 mm). If a smaller or larger FE size is to be used, the softening part of the σ-ε response will require some adjustment, as the fracture energy should remain unchanged. For example: for a smaller element size the area under the softening part of the σ-ε response needs to be increased until the product of the element width and the calculated area equals the fracture energy for element size of 150 x 150 mm. An element size of 150 x 75 mm, i.e., the element to the right of the loads in Fig.9, would dissipate double of the fracture energy upon complete cracking compared to 150 x 150 mm element. Since half of the beam is modelled, only half of its energy will be dissipated during the analysis, therefore, the use of an element size of 150 x 75 mm with the tensile σ-ε response of Fig.10 is justifiable. The appropriateness of finer mesh is investigated by using finite elements measuring 37.5 x 37.5 mm and the tensile σ-ε response shown in Fig. 10. The results indicated a relatively large discrepancy between experimental and calculated P-δ responses especially beyond the crack point (refer to Fig.11).

The inverse analysis showed that compressive strains exceeded the elastic limit ($\varepsilon_{c0}=1.6 \times 10^{-3}$) only for deflections greater than 3 mm, i.e., a serviceability limit prescribed by the Japanese Institute of Concrete procedure (1983). Accordingly, within the desired practical part of the P-δ response, the behaviour was dominated by cracking while the compression side remained elastic. A linear elastic compressive σ-ε response is deemed to be sufficient for the FEA of this beam.

Results of the finite element analysis

In Fig.11 the computed P-δ response obtained using the developed FE model is compared to the experimental results. The computed P-δ response is generated by plotting double the sum of the reactions at loading points versus the vertical (Z-direction) deflection at the nodes of the symmetry line for the consecutive increments. The computed and the measured P-δ responses show a reasonable correlation.

Fig.12 shows the distribution of the strains and stresses through the depth of the analyzed SFRC beam. The linear strain distribution correlates well with the assumption made for the numerical method used to back-calculate the tensile σ-ε relationship. The stress distribution shows that the σ-ε relationship is reasonably represented through the depth of the beam. The analysis also shows that no plastic deformation has taken place in the compression side of the beam as the compressive strain and stress values are below the limits of 1.6×10^{-3} and 45 MPa, respectively. This affirms the result obtained from the inverse analysis and correlates well with the findings of the study conducted by Robins et al. (2001).

Fig.13 shows the comparison between the input and the output tensile σ-ε responses extracted at the integration point (I_a) with respect to the layers 11 and 10 through the depth of the beam (refer to Fig.9). At the integration point, the output and the input responses are found to correlate well up to a point. For the layer 11 in the part of the curve beyond tensile strains of 0.004, the input and output tensile σ-ε response diverge. This seems to be caused by the numerical simulation used in which the direction of the crack is fixed once the crack initiates (single-fixed crack approach). It is worth noting that the peak load on the P-δ response corresponds to a tensile stress located in the softening part of the σ-ε relationship between ε_{t0} and ε_{t1}. This supports the findings described in Fig.7 and Fig.10.

The tensile stress in the elements to the left of the loading point were found to be less than the cracking stress at integration points named as (I_b) and (I_c). This indicates that the boundary value problem has enforced localisation of the crack in a single column of elements; therefore, the prescribed fracture energy is indeed dissipated computationally.

Summary and conclusions

The method presented here can be used to back-calculate tensile σ-ε using measured M-ϕ or P-δ responses obtainable with minimal testing complexities compared to stresses and strains. In addition, the method utilizes a macro approach, whereby, the influence of the steel fibre parameters and the concrete matrix are reflected in the measured M-ϕ or P-δ responses. This is of a considerable advantage compared to procedures utilizing a micro approach in which the

fibre properties, the concrete matrix properties and the fibre-matrix interaction have to be known.

The back-calculated σ-ε response can be utilized in a NLFEA to model the behaviour of SFRC beams. The σ-ε response calculated using the developed numerical method is mesh size dependent. The area under the softening part of the σ-ε response is mostly dependent on the width of the element that lies between the applied loads in the third-point beam test used in the analysis. For NLFEA, the size of the FE should be selected based on this width, however, adjustments to the softening part are necessary if a smaller or larger FE size is used.

The single fixed crack approach is found to be sufficiently accurate to model the cracking behaviour of the SFRC beams up to a serviceability deflection limit.

The analysis confirmed that the point where the material first reaches its maximum tensile stress occurs in the pre-peak regions of both the M-ϕ and P-δ responses. Hence, the analysis should proceed beyond the cracking stress in order to appropriately evaluate the load-carrying capacity of the SFRC structures.

The maximum compressive stress in the beam falls within the linear elastic zone. The assumption of a linear-elastic compression σ-ε response is adequate for these SFRC structural members subject to flexure.

Notations

The following symbols are used in this paper:

A	=	Area of beam cross-section.
E_c	=	Young's modulus for of the SFRC.
F	=	Total force on a beam cross-section.
G	=	Shear modulus.
I	=	Second moment.
I_a	=	Integration point of a finite element.
L	=	Span of the beam.

M	=	Moment.
M_c	=	Moment on the descending part of the moment-curvature relationship.
M_L	=	Moments due to actual load.
M_m	=	Maximum moment.
M_u	=	Moment due to a unit load.
P	=	Vertical load.
V	=	Shear force.
V_c	=	Shear force at any point on the shear force-shear strain relationship.
V_L	=	Shear forces due actual load.
V_m	=	Maximum shear force.
V_u	=	Shear force due to a unit load.
X , Y, and Z	=	Orthogonal directions.
a	=	Depth of neutral axis.
b	=	Width of a beam.
dx, dy	=	Length and width of differential element.
f_{sh}	=	Form factor for shear (equals 6/5 for rectangular section).
h	=	Depth of a beam.
y	=	Variable representing the depth from neutral axis.
Δ_X, Δ_Y and Δ_Z	=	Displacement in the X, Y, and Z directions, respectively.
γ	=	Shear strain.
γ_c	=	Shear strain at any point on the shear force-shear strain relationship.
γ_m	=	Maximum shear strain.
δ	=	Deflection of elevated beam or slab.
δ_m	=	Deflection due to moment.
δ_V	=	Deflection due to shear.
ε	=	Strain.
ε_{bot}	=	Tensile strain at bottom ligament of the beam cross-section.
ε_{c0}	=	Elastic limit for compressive strain.
ε_{cu}	=	Ultimate compressive strain.

ε_{t0} = Cracking strain.

ε_{t1} = Residual strain.

ε_{top} = Compressive strain at top ligament of the beam cross-section.

ε_{tu} = Ultimate tensile strain.

θ_X, θ_Y and θ_Z = Rotation in the X, Y and Z directions, respectively.

λ = Slope of the second softening part of the tensile stress-strain curve.

σ = Stress.

σ_{cu} = Compressive strength of SFRC.

σ_{t0} = Cracking strength of a composite material.

σ_{tu} = Residual stress.

ϕ = Curvature.

ϕ_c = Curvature on the descending part of the moment-curvature relationship.

ϕ_m = Curvature corresponding to the maximum moment (M_m).

ψ = Slope of first softening part of the tensile stress-strain curve.

References

Alena, K., Kristek, V., and Broukalova, I. (2004). Material Model of FRC - Inverse Analysis. Proceedings of the 6th International RILEM Symposium, Varrena / Italy. PP 857-864.

Banthia, N., Chokri, K., and Trottier, J.F. (1995). Impact Tests on Cement-Based Fiber Reinforced Composites. Publications of the American Concrete Institute, SP.155-9, Detroit / United States of America. PP 171-188.

Bekaert, (1999). Steel Fibers for the Pre-cast Industry. Bekaert NV. Dramix® Technical Pamphlet.

Dupont, D. And Vandewalle, L. (2003). Modelling with a Stress-Strain Approach. Proceedings of the International Symposium: Role of concrete in Sustainable Development, Dundee/ Scotland, PP 103-112.

Elsaigh, W.A. (2001). Steel Fibre Reinforced Concrete Ground Slabs. M.Eng. Dissertation, University of Pretoria / South Africa.

Elsaigh, W.A. (2007). Modelling the Behaviour of Steel Fibre Reinforced Concrete Ground Slabs. Ph.D. Dissertation, University of Pretoria / South Africa.

Elsaigh, W.A., Robberts, J.M., and Kearsley, E.P. (2004). Modelling Non-linear Behaviour of Steel Fibre Reinforced Concrete. Proceedings of the 6th International RILEM Symposium, Varenna / Italy. PP 837-846.

Gere, J.M., and Timoshenko, S.P. (1991). Mechanics of Materials. 3rd edition. ISBN 0412-368803.

Japanese Concrete Institute (1983). Standards for Test Methods of Fibre Reinforced Concrete. Method JCI-SF4.

Jindal, R.L. (1984). Shear and Moment Capacities of Steel Fibre Reinforced Concrete Beams. International Symposium, American Concrete Institute, Detroit / United States of America. PP1-16.

Johnston, C.D. (1985). Toughness of Steel Fibre Reinforced Concrete. Proceedings of the Steel Fibre Concrete US-Sweden Joint Seminar (NSF-STU), Swedish Cement and Concrete Research Institute, Stockholm / Sweden. PP 333-360.

Johnston, C.D., and Zemp, W.R. (1991). Flexural Fatigue Performance of Steel Fibre Reinforced Concrete: Influence of Fibre Content, Aspect Ratio, and Type. American Concrete Institute, Material Journal, V. 88, No. 4. PP 374-383.

Lim, T.Y., Paramasivam, P., and Lee, S.L. (1987a). Analytical Model for Tensile Behaviour of Steel-fibre Concrete. American Concrete Institute, Materials Journal, V. 84, No. 4. PP 286-298.

Lim, T.Y., Paramasivam, P., and Lee, S.L. (1987b). Bending Behaviour of Steel-fibre Concrete Beams. American Concrete Institute, Structural Journal, V. 84, No. 4. PP 524-536.

Lok, T-S., and Xiao J-R. (1998). Tensile Behaviour and Moment-Curvature Relationship of Steel Fibre Reinforced Concrete. Magazine of Concrete Research, No. 4. PP 359-368.

MathSoft (2001), Mathcad 2001i, MathSoft International, (Knightway House, Park Street, Bagshot, GU19 5AQ), United Kingdom.

Minelli, F., and Vecchio, F.J. (2006). Compression Field Modelling of Fibre-Reinforced Concrete Members Under Shear Loading. American Concrete Institute, Structural Journal, V.103, No. 2. PP 244-252.

MSC.Marc (2003). Mentat V. 2003, MSC. Software Corporation, 2 Mac Arthur place, Santa Ana, CA92707. United State of America.

Nemegeer, D. (1996). Design Guidelines for Dramix® Steel Wire Fibre Reinforced Concrete. Indian Concrete Journal, V.70, No.10. PP 575-584.

Olesen, J.F. (2001). “Fictitious Crack Propagation in Fibre-Reinforced Concrete Beams”. Journal of Engineering Mechanics, V. 127, No. 3. PP 272-280.

Parker, F.Jr. (1974). Steel Fibrous Concrete for Airport Pavement Applications. U.S. Army Engineer Waterways Experiment Station. Federal Aviation Administration, Washington DC / United States of America, Technical Report No. S-74-12. 205 P.

Østergaard, L., and Olesen, J.F. (2005). “Method for Determination of Tensile Properties of ECC I: Formulation and Parameter Variations”. Proceedings of the International Workshop on High Performance Fibre Reinforced Cementitious Composites in Structural Applications, Task Group A: Standards for Materials and Testing, Honolulu / Hawaii. PP 60-67.

Østergaard , L., Walter, R., and Olesen, J.F. (2005). “Method for Determination of Tensile Properties of ECC II: Inverse Analysis and Parameter Variations”. Proceedings of the International Workshop on High Performance Fibre Reinforced Cementitious Composites in Structural Applications, Task Group A: Standards for Materials and Testing, Honolulu / Hawaii. PP 68-74.

RILEM TC 162-TDF, (2002). “Test and Design Methods for Steel Fibre Reinforced Concrete: Bending test - Final Recommendation”. Journal of Materials and Structures, V.35. PP 579-582.

Robins, P., Austin, S., Chadler, J., and Jones, P. (2001). “Flexural Strain and Crack Width Measurement of Steel-Fibre-Reinforced Concrete by Optical Grid and Electrical Gauge Methods”. Cement and Concrete Research (31). PP 719-729.

Soroushian, P., and Bayasi, Z. (1987). “Prediction of the Tensile Strength of Fibre Reinforced Concrete: A Critique of the Composite Material Concept”. Proceedings of the American Concrete Institute - Fibre Reinforce Concrete: Properties and Applications. SP 105.

Tlemat, H., Pilakoutas, K., and Neocleous, K. (2006). “Modelling of SFRC Using Inverse Finite Element Analysis”. Journal of Materials and Structures, RILEM, V. 39 Issue 6. PP 221-233.

Vandewalle, L. (2003). Design with σ-ε Method. Proceedings of the RILEM TC 162-TDF Workshop: Test and Design Methods for Steel Fibre Reinforced Concrete-Background and Experience, Bochum / Germany, 207 P.

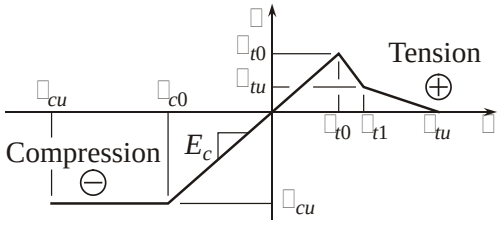

Fig.1: Proposed σ-ε response.

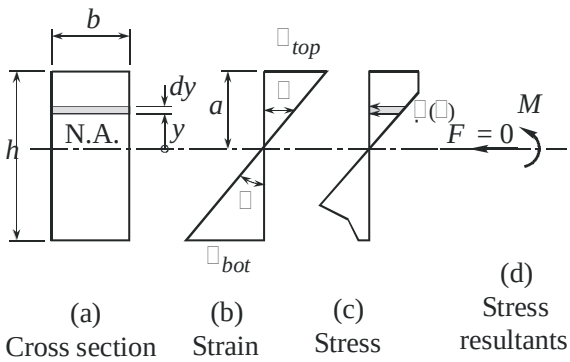

Fig.2: Stress and strain distributions at a section.

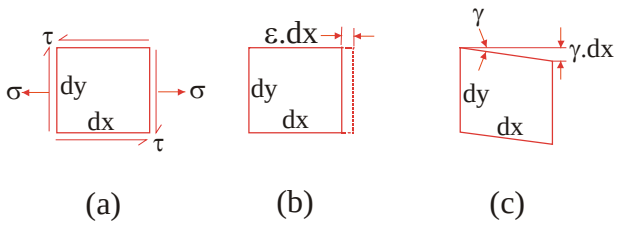

Fig.3: Differential element from the beam.

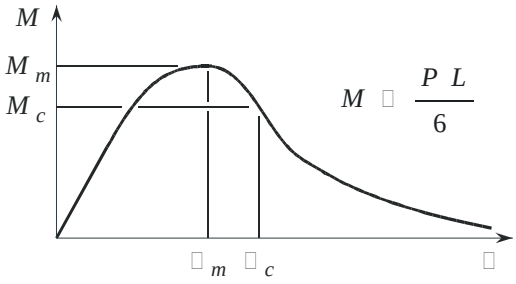

(a) Moment-curvature relationship

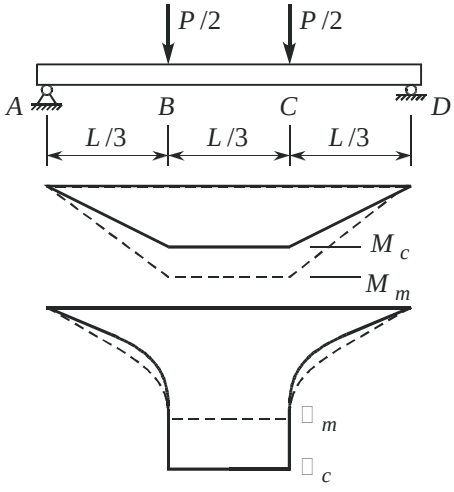

(b) Moment and curvatures distributions for an applied load P

Fig.4: Determination of the M-ϕ distribution along the beam.

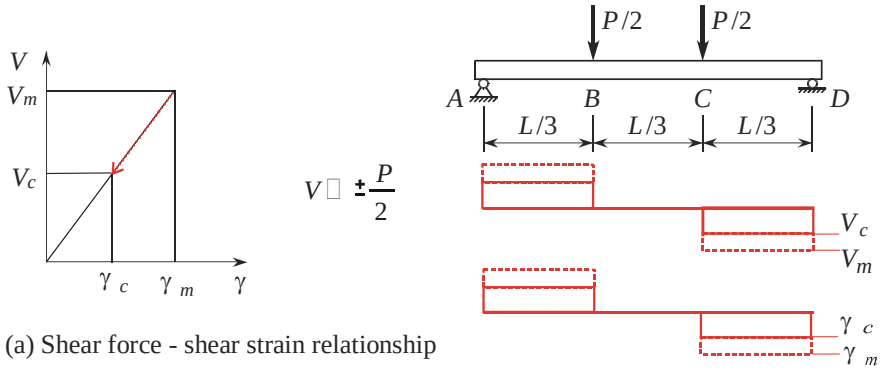

(a) Shear force - shear strain relationship

(b) Shear forces and shear strain distributions for an applied load P

Fig.5: Determination of the shear-shear strain distribution along the beam.

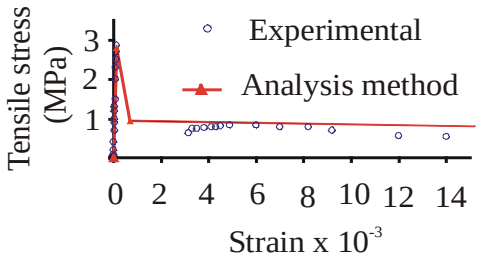

Fig.6: Calculated tensile σ-ε response to experimental results of Lim et al. (1987 b).

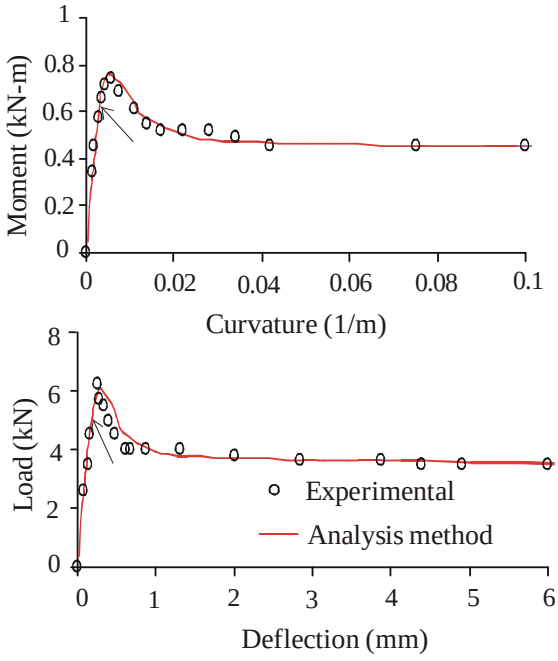

Fig.7: Experimental (Lim et al., 1987 a) and calculated M-ϕ and P-δ responses.

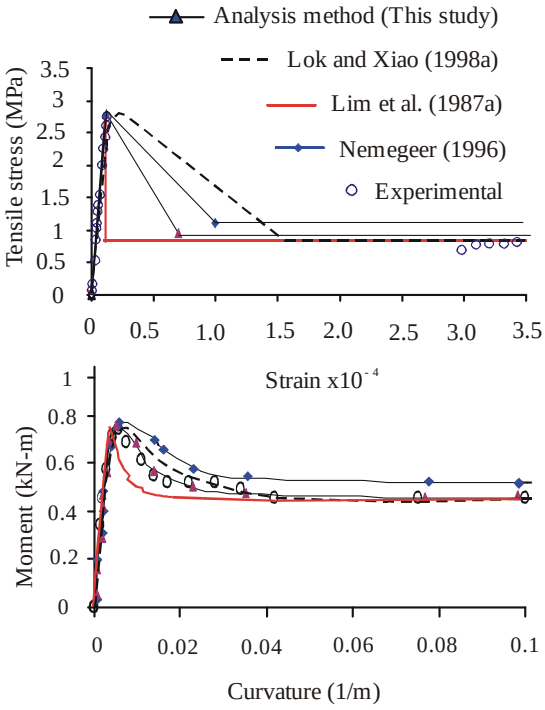

Fig.8: Correlation between tensile σ-ε responses determined using various models.

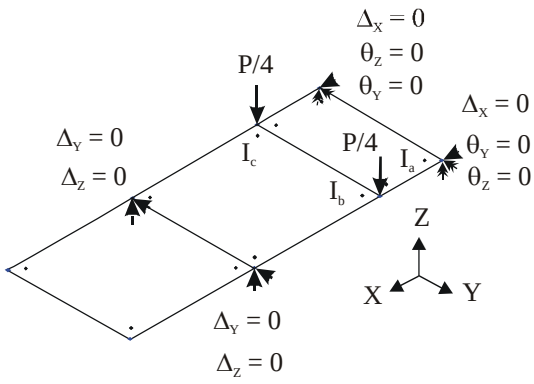

Fig.9: Mesh and boundary conditions for beam.

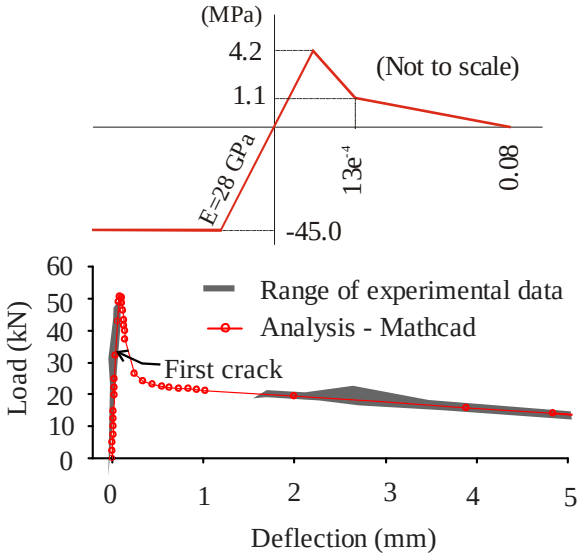

Fig.10: σ-ε and P-δ responses for SFRC containing 15 kg/m^3 hooked-end steel fibres.

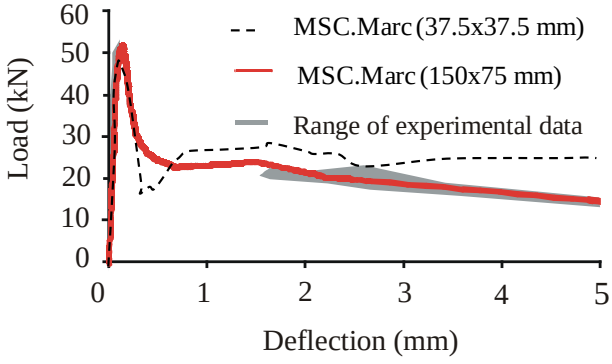

Fig.11: Comparison between NLFEA and measured P-δ responses.

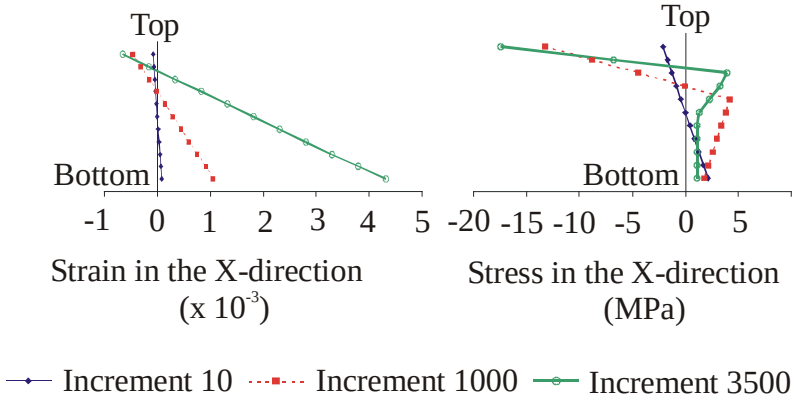

Fig.12: Distribution of the strains and stresses through the depth of the beam.

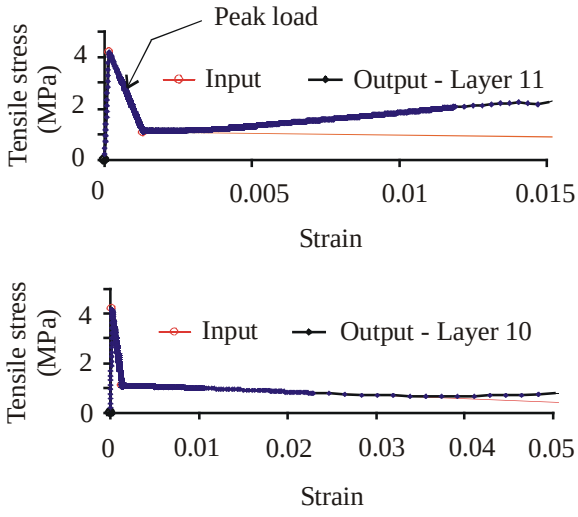

Fig.13: Comparison between input and output tensile σ-ε responses.